Solar RRL

WILEY VCH

Solar RRL

RESEARCH ARTICLE

Compositional and Defect Engineering of Metal Halide Perovskite-Based Heterojunctions for Efficient Nitrogen Photofixation

Costanza Tedesco[1] | Angelica Simbula[2] | Riccardo Pau[2] | Francesca Merlo[1] | Andrea Speltini[1] | Vincenza Armenise[3] | Andrea Listorti[4] | Luca Gregori[5] | Asma A. Alothman[6] | Edoardo Mosconi[6,7] | Michele Saba[2] | Antonella Profumo[1] | Lorenzo Malavasi[1]

[1]Department of Chemistry and INSTM, University of Pavia, Pavia, Italy | [2]Department of Physics, University of Cagliari, Monserrato, Italy | [3]CNR NANOTEC—c/o Dipartimento di Chimica, Università di Bari, Bari, Italy | [4]Department of Chemistry, University of Bari "Aldo Moro", Bari, Italy | [5]Department of Chemistry, Biology and Biotechnology, University of Perugia and INSTM, Perugia, Italy | [6]Chemistry Department, College of Science, King Saud University, Riyadh, Kingdom of Saudi Arabia | [7]Computational Laboratory for Hybrid/Organic Photovoltaics (CLHYO), Istituto CNR di Scienze e Tecnologie Chimiche "Giulio Natta" (CNR-SCITEC), Perugia, Italy

Correspondence: Lorenzo Malavasi (lorenzo.malavasi@unipv.it)

Received: 30 October 2024 | **Revised:** 16 December 2024 | **Accepted:** 28 January 2025

Funding: PON Ricerca e Innovazione, Grant/Award Number: 2014–2020 REACT-EUDM 1062 2021project N. 04-G-14266-–1; Centro Servizi Ateneo per la Ricerca (CeSAR) of University of Cagliari; Italian Ministry for University and Research (MUR), Grant/Award Number: PRIN 2022 CUP F53D23005090006PRIN 2022 F53D23001050006; National Recovery and Resilience Plan (NRRP), Grant/Award Number: Project "Network 4 Energy Sustainable Transition—NEST", Spoke 1, Project code PE0000021; MUR (PRIN 2022 2022YM3232 – NanoPix and PRIN 2022 PNRR P2022ZYTJY—Master); Italian Ministry of University and Research (MUR) (National Recovery and Resilience Plan (NRRP), Mission 4, Component 2, Investment 1.1, Call for tender No. 104 published on 2.2.2022); National Recovery and Resilience Plan (NRRP); European Union—NextGenerationEU—(Project Title "Towards efficient and cost-effective nitrogen fixation via photocatalysis: insights from experiment and theory—PHOTOFIX—CUP F53D23005160006 - Grant Assignment Decree No. 1064 on 18.7.2022); King Saud University, Riyadh, Kingdom of Saudi Arabia (Distinguished Scientist Fellowship Program (DSFP))

Keywords: computational modelling | green ammonia | heterojunction | metal halide perovskite | nitrogen photofixation | photocatalysis

ABSTRACT

Designing innovative photocatalysts for nitrogen photofixation is becoming crucial for the development of carbon-neutral ammonia production. Metal halide perovskites (MHPs) provide a rich library of materials with an easy tuning of the semiconductor bandgap in order to integrate them in devices with different functionalities. An under-explored path is their exploitation to run a wide range of photoredox reactions mediated by solar light. Herein, heterojunction is developed based on the vacancy-ordered double-perovskite Cs_2SnBr_6 and carbon nitride nanosheets and demonstrate its ability in running the nitrogen photofixation reaction to produce ammonia under solar light. An investigation is done on full Cs_2SnBr_6/g-C_3N_4 system and an optimal range providing an outstanding ammonia evolution rate up to 270 $\mu mol\ g^{-1}\ h^{-1}$is identified, which is quantified by means of ion selective electrode. Mechanistic insight into the photofixation reaction is obtained through a combination of advanced spectroscopy and computational modeling. Efficient ammonia production stems from an effective charge transfer from the perovskite to the nitrogen vacancies on the carbon nitride enabled by the proposed absence of self-trapped excitons in Cs_2SnBr_6, which also provides additional reactive sites through bromide vacancies. This work paves the way to MHP-based catalyst design strategy for sustainable ammonia production.

1 | Introduction

The utilization of NH_3, obtained through nitrogen fixation, as a green alternative fuel and chemical, represents a significant promise in mitigating carbon emissions and reaching energy independence [1–3]. In particular, the potential of ammonia as an energy vector lies in its ability to store and transport energy efficiently: it can be exploited to release hydrogen, to generate

electricity in fuel cells, or directly as a fuel in internal combustion engines, already resulting in the development of ammonia-fueled engines for transport and power generation [2–4]. The current Haber-Bosch process used to produce ammonia is energy-consuming requiring high temperatures (>500°C) and extremely high pressure (200–300 bar) and accounts for over 1% of total global fossil energy and for 11% of the energy consumed in chemical industries [1, 5]. Photofixation of nitrogen for ammonia production, on the contrary, is a sustainable process leveraging the energy from sunlight to convert atmospheric nitrogen (N_2) into ammonia (NH_3), with the aid of photocatalysts to harness sunlight and drive the reduction of nitrogen to ammonia [6–8]. Although the fixation of N_2 to NH_3 is thermodynamically convenient, being the triple bond in N_2 extremely strong, the reaction cannot occur spontaneously under ambient conditions [3]. Moreover, low solubility and slow diffusion of nitrogen in water are significant impediments for enhancing the efficiency of the process. The last step of nitrogen photofixation involves the progressive reduction of nitrogen atoms by the electrons to form ammonia, typically in the presence of a hydrogen source such as water [4, 5].

The efficiency of photofixation, as in general for photocatalytic processes, largely depends on the choice of the photocatalysts. In addition to the common requirements of effective photocatalytic materials, the presence of defects such as nitrogen, oxygen, and sulfur vacancies, acting as reactive sites for N_2 adsorption, is pivotal for nitrogen photofixation [4, 5, 9]. Currently, metal oxides and graphitic carbon nitride (g-C_3N_4), commonly used in several photocatalytic reactions, have been as well investigated to run nitrogen reduction reaction to NH_3 [2, 3]. Together with doped TiO_2 and ZnO nanocrystals, the possibility of introducing oxygen vacancies greatly boosted the performance of BiOX (X = Cl, Br,I) oxyhalide compounds, which present intense visible light activity (bandgap from 2.4 to 3 eV) [7–10, 10–15]. Recently, bio-inspired sponge systems based on BiOBr with oxygen vacancies achieved more than 2 mmol $g^{-1}h^{-1}$ of ammonia evolution rate [8]. At the same time, to overcome the rapid carrier recombination rate of carbon nitride, several strategies have been developed, and the introduction of foreign elements such as metals (e.g., Fe, Co) or non-metals (e.g., S, P) into the g-C_3N_4 matrix effectively enhanced its electronic properties and improve charge separation [16–18]. For the nitrogen photofixation reaction the combination of g-C_3N_4 with other materials, such as metal oxides or conducting polymers, through the realization of heterojunctions, can synergistically enhance photocatalytic activity and stability promoting good ammonia production rates [6, 16, 19–21]. Among other approaches, the generation of nitrogen vacancies in carbon nitride shows to be a good strategy to boost the nitrogen photofixation as demonstrated in recent times.

While the previously reported materials could represent potential good candidates, their wide bandgap, high carrier recombination rates, and relative difficult manipulation of their defect chemistry, suggest that novel materials and approaches should be discovered. In this respect, in the last years, metal halide perovskites (MHPs) have demonstrated to be efficient and promising materials for various photocatalytic applications thanks to their unique features such as tunable bandgap, high absorption coefficient, and long charge carrier lifetime and diffusion lengths, which are crucial for reducing recombination rates and enhancing photocatalytic efficiency [22–25]. While MHPs have been extensively explored for several solar-related applications, such as photocatalytic H_2 generation, photoreduction of CO_2, and synthesis of organic molecules, their exploitation in the field of nitrogen photofixation is in its newborn era and the full exploitation of their potential for nitrogen photofixation has still to be demonstrated [26]. In this article, we aimed at engineering optimized perovskite-based heterojunctions for nitrogen photofixation that could provide high production rates and where the perovskite could itself provide active sites for the nitrogen reduction to ammonia.

On these bases, we report here a novel heterojunction for nitrogen photofixation based on the vacancy-ordered Cs_2SnBr_6 perovskite and g-C_3N_4 nanosheets showing efficient green ammonia production rates (up to ≈270 μmol g^{-1} h^{-1}) and where the perovskite, thanks to its peculiar crystal and electronic structure, can actively participate in the photofixation reaction. Through a combined experimental and computational work, we were able to provide a detailed picture of the mechanism underpinning the efficient nitrogen reduction reaction to ammonia observed in this system that can be used to further expand this novel applicative field of photoactive perovskites.

The Cs_2SnBr_6/g-C_3N_4 system has been synthesized according to the experimental procedure reported in the Supporting Information (SI). Weight ratios between Cs_2SnBr_6 and g-C_3N_4 nanosheets investigated are (wt% of perovskite) 100, 80, 65, 50, 45, 35, 20, 15, 7, and 0.

Figure 1a reports the room temperature X-ray diffraction (XRD) patterns of some selected compositions investigated. Bottom part of Figure 1a shows the pattern of Cs_2SnBr_6 vacancy-ordered double perovskite, which is also reported against the calculated pattern in Figure 1b. The perovskite displays a cubic symmetry with *Fm*-3*m* space group (#225) and a lattice parameter of 10.7761(2) Å, in agreement with previous results [27]. A sketch of the cubic unit cell is reported in Figure 1c. At the top of Figure 1a, the X-ray pattern of pure g-C_3N_4 nanosheets is reported. The typical broad peaks around 13° and 28° corresponding to the (100) and (002) reflections are clearly visible. In all the patterns of the composites (cf. Figure 1a) the diffraction peaks of Cs_2SnBr_6 are clearly visible due to its high scattering power with respect to g-C_3N_4. Morphological inspection of Cs_2SnBr_6, g-C_3N_4, and selected composites has been carried out by scanning electron microscopy (SEM) and the results are reported in Figure S1. g-C_3N_4 nanosheets have also been characterized by transmission electron microscopy (TEM) and representative images showing their nanostructure are shown in Figure S2. Elemental mapping through energy-dispersive X-ray spectroscopy (EDS) has been carried out for the composite with 35 wt% of Cs_2SnBr_6, as an illustrative example, and is reported in Figure S3, confirming the formation of a composite between the two semiconductors. Electron paramagnetic resonance (EPR) measurements have been carried out on g-C_3N_4 nanosheets to confirm the presence of nitrogen vacancies, which are characterized by the presence of a peculiar signal centered around $g = 2$, as shown in Figure S4, due to the presence of unpaired electrons [28].

Figure 2a reports the results in terms of ammonia evolution rates as a function of Cs_2SnBr_6 amount, expressed as μmol g^{-1} h^{-1},

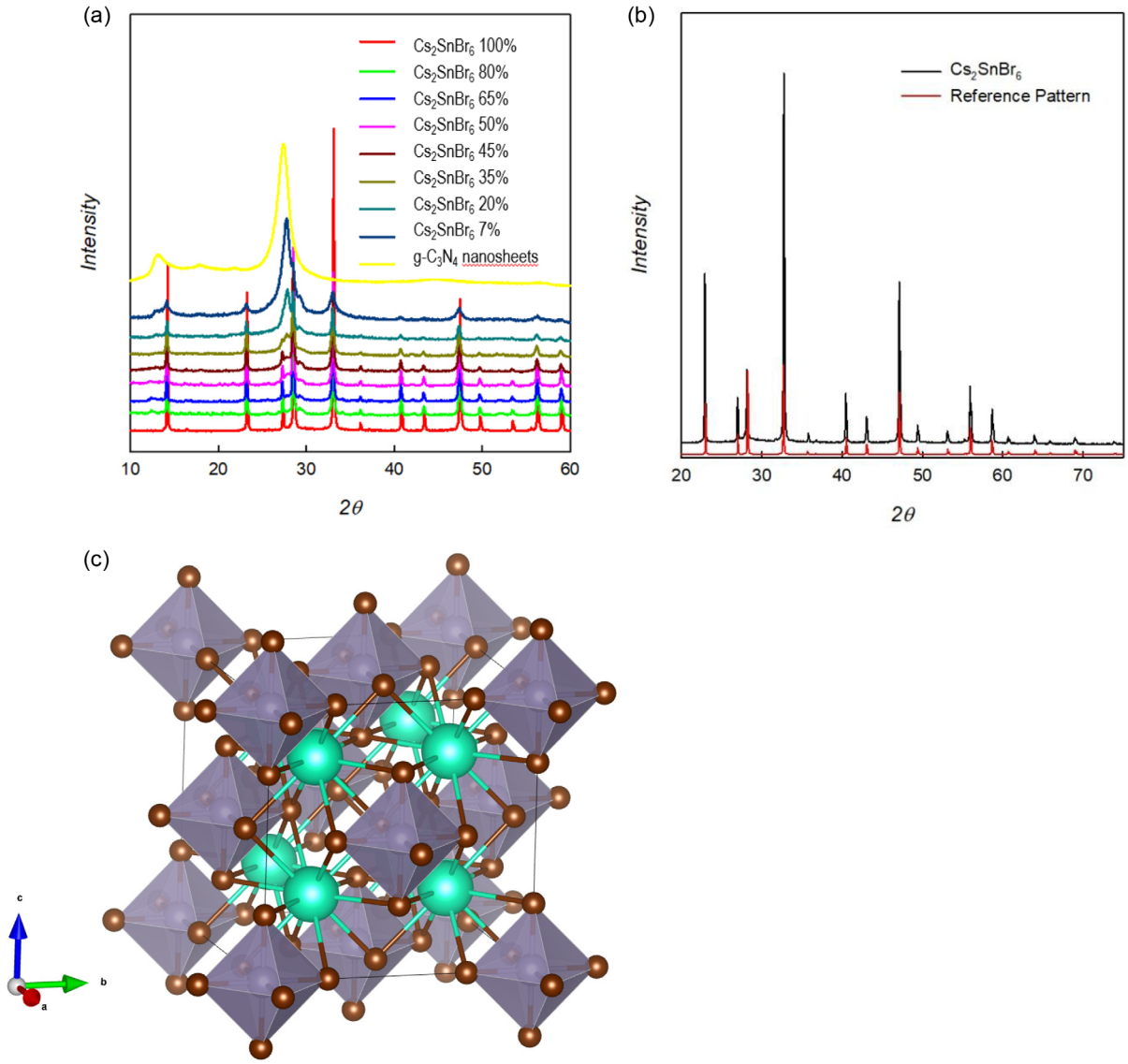

FIGURE 1 | (a) XRD pattern of Cs_2SnBr_6/g-C_3N_4 composites; (b) XRD pattern of Cs_2SnBr_6 against the reference cubic structure, and (c) sketch of Cs_2SnBr_6 crystal structure where Cs^+ ions are shown as green spheres and the bromide ions as grey spheres included into the octahedra.

obtained by photocatalytic experiments under simulated solar light. Experimental details are provided in the SI for both the photocatalytic experiments and ammonia determination, which is based on ion selective electrode quantification instead of colorimetric methods (which tend to overestimate the actual concentrations), thus providing a more accurate and interferent-free approach [26].

The trend of ammonia evolution rate steeply increases from pure Cs_2SnBr_6 (about 50 $\mu mol\, g^{-1}\, h^{-1}$) to >200 $\mu mol\, g^{-1}\, h^{-1}$ for the composites including an intermediate amount of perovskite (20–25%) and reaching the highest value of 266 $\mu mol\, g^{-1}\, h^{-1}$ for the composition Cs_2SnBr_6 35 wt%/g-C_3N_4 65 wt% before decreasing for composites with a larger amount of g-C_3N_4. Note that pure g-C_3N_4, under these reaction conditions, provides an ammonia evolution rate of 2.7 $\mu mol\, g^{-1}\, h^{-1}$.

The data reported in Figure 2a demonstrate, first of all, that the perovskite alone is already quite active in the nitrogen reduction reaction and that such activity can be boosted through the heterojunction formation, achieving a value, for the optimal composition, which is about four times that of pure Cs_2SnBr_6. The absolute value of ammonia production obtained for the Cs_2SnBr_6 35 wt%/ g-C_3N_4 65 wt% composition is nearly eight times larger than what previously reported on perovskite-based systems [29]. The good stability of the ammonia production has been tested on the top performing composite for three successive cycles as reported in Figure 2b. Post-catalysis XRD data are shown in Figure S5, indicating the stability of the system.

UV-Vis absorption spectra and the corresponding Tauc plots for Cs_2SnBr_6/g-C_3N_4 system are reported in Figure S6. The bandgap of Cs_2SnBr_6 is 2.75 eV and that of g-C_3N_4 is 2.78 eV, in agreement with previous reports [26, 27]. Being the two bandgaps very close, no relevant shifts or trend are observed as a function of composition. The normalized photoluminescence spectra of the Cs_2SnBr_6/g-C_3N_4 system are reported in Figure 3. The emission is dominated by the broad and intense features of graphitic

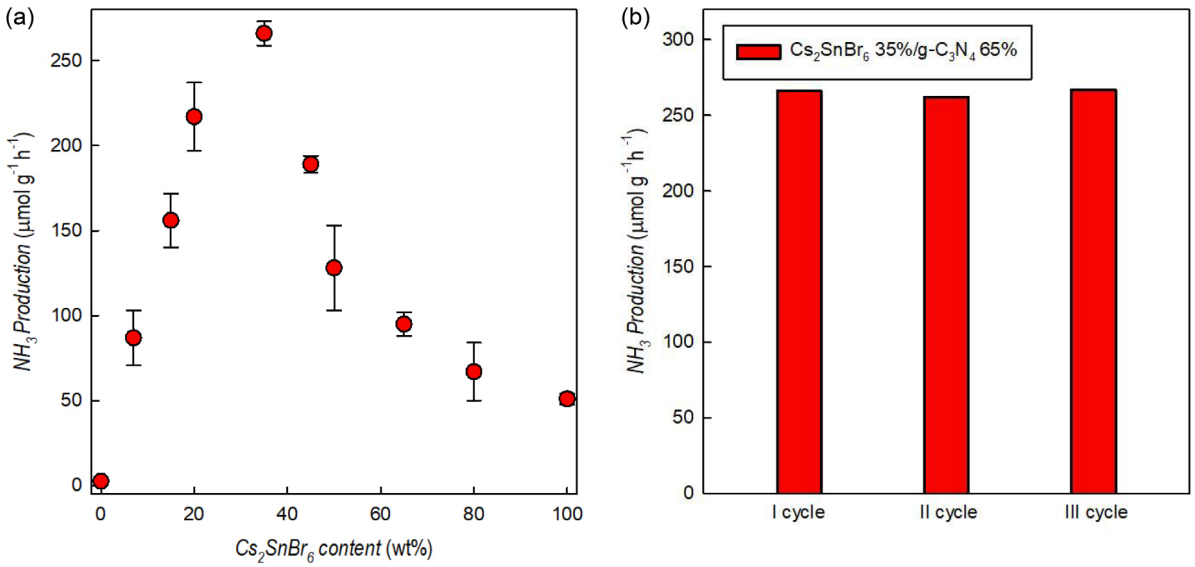

FIGURE 2 | Ammonia photocatalytic production: (a) as a function of Cs_2SnBr_6 wt% in the composites. ($n = 3$, simulated solar light, 500 W m^{-2}); (b) as a trend over three cycles for the best performing composite, namely Cs_2SnBr_6 35 wt%/ g-C_3N_4 65 wt%.

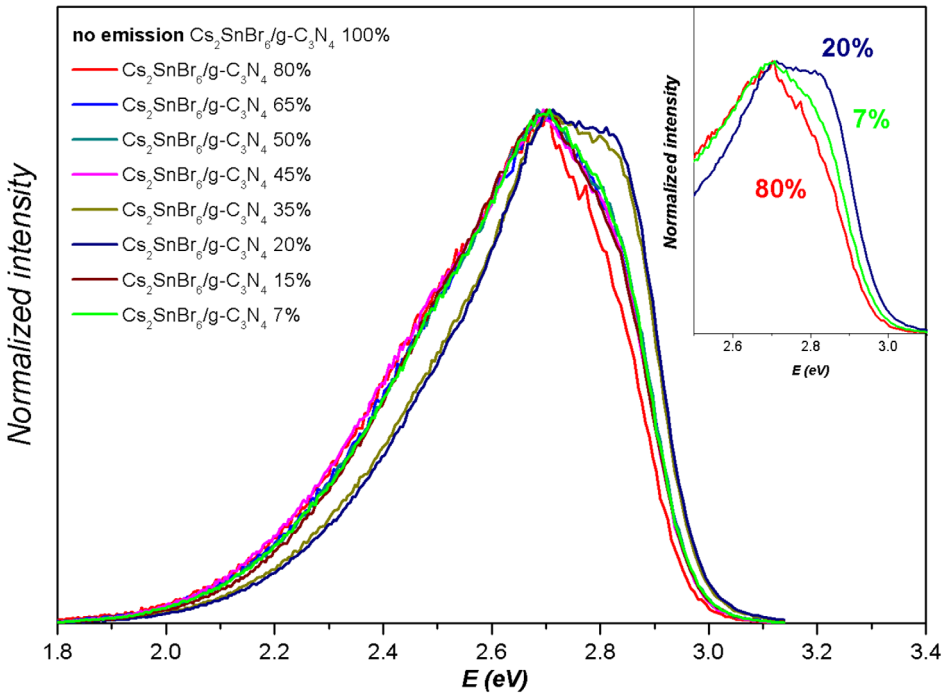

FIGURE 3 | Emission spectra of Cs_2SnBr_6/g-C_3N_4 composites powders at different percentages of Cs_2SnBr_6 loading (wt%). $\lambda_{ex} = 375$ nm. Inset: zoom on a relevant spectral zone (see text for details).

carbon nitride, even at very high perovskite loading. Such broad spectra, that completely covers the weak perovskite emission, derive from the superimposition of multiple electronic transitions [30]. In particular, three transitions have been modeled in pristine g-C_3N_4: a high-energy one, centered at around 2.81 eV, which derives from the relaxation of δ* electrons to the LP state, and two low energy transitions centered at 2.70 and 2.42 eV. To access these low-energy transitions a non-radiative mechanism to populate the π^* state is required, thus the structure of the broadband spectrum depends on the efficiency of this process. In previous works, the interplay between the density of defects and the non-radiative population of π^* state have been studied and related to the photocatalytic properties of g-C_3N_4 [30].

A close inspection of the spectral region around the emission band peak (inset of Figure 3) shows that, for low perovskite loadings, there is an increase of low-lying sub-band population, as the emission displays a reduced contribution from the high-energy transition. Conversely, by increasing the perovskite content, the high-energy transition (2.81 eV) became more and more pronounced, with a peak around 20% (and 35%, see main Figure 3) of

perovskite content while the trend inverts after this value and, at higher perovskite loadings, one can observe again a reduced contribution to the emission band from the high-energy transition. Very interestingly, the trend of the high-energy transition intensity as a function of perovskite loading recalls that of the ammonia production reported in Figure 2, with the maximum values of the photocatalytic activity found in the range 20%–35% of perovskite corresponding to the percentages that lead to a higher contribution to the broad band by the δ* → LP state transition. This observation points out the effect of compositional engineering in funneling optical excitations to the sites where they can be exploited in photocatalytic processes. In a recent work on MHP/g-C_3N_4, we demonstrated that the reduction of the low-lying sub-band population allows to retain the excitation in the carbon nitride component where it can be exploited for the ammonia production [26]. Herein, we further corroborate this observation and, moreover, we also underline an active role of perovskite in offering catalytic centers as it will be confirmed by the computational modeling work. Noticeably, in these composite systems, a very simple and fast checking of the steady-state photoluminescent properties allows to conveniently assess composition/performances relations.

To understand the excited state dynamics as a function of Cs_2SnBr_6/g-C_3N_4 composition, differential transmission (DT) measurements were performed. Excitation of solutions in quartz cuvettes was provided by a femtosecond pulsed laser at 350 nm, and the transient transmission signal was collected in a pump and probe configuration with sub-ps resolution (details about experimental method in SI). A set of data extracted from the measurements are shown in Figure 4a, where DT spectra are reported for the different compositions, from 100% g-C_3N_4 (black line) to 100% Cs_2SnBr_6 (green line). By observing the two photobleaching features centered at 500 nm and 630 nm, it is worth noticing that the intensity of transitions changes substantially with the change in composition. First of all, lower overall DT signal amplitude is obtained from the pure compounds, which are also the ones with lower ammonia evolution rates. When adding small amounts of perovskite to the g-C_3N_4 the intensity of the signal is boosted, analogously to what already observed for the ammonia production rate in Figure 2 and, correspondingly, a broad DT peak centered around 630 nm rises. When the perovskite amount surpasses 40%, the amplitude of the DT signal decreases down to the pure perovskite case.

Another interesting piece of information that can be extracted from DT measurements is the fact that DT spectra of composites with increased evolution rates (particularly from 7% to 35% perovskite content) have the same spectral features of pure g-C_3N_4, suggesting that the reaction occurs mainly at the g-C_3N_4 defect sites, with an introduction of an amount of perovskite <40% favoring the charge transfer towards g-C_3N_4 sites. The time evolution of the signal is reported in Figure S7, showing that, after a first initial decay on a picosecond scale, the signal stabilizes and follows a much slower decay. To get a complete overview of the data, in Figure 4b are reported the integrated DT signals for different wavelength ranges and compositions. A fairly good agreement is found between the trend of the DT signals and that of the ammonia generation reported in Figure 2.

Time resolved photoluminescence emitted by the composites was also investigated and the results are reported in Figure 5: here the time decays show that compounds with low-intermediate perovskite amounts, corresponding to high ammonia production rates, have longer TRPL lifetimes. This suggests that for these compositions there is some degree of suppression of nonradiative decays for photoexcited carriers, with a lifetime longer than that of both pure Cs_2SnBr_6 and pure g-C_3N_4.

To gain insight into the electronic properties and photocatalytic mechanism, we have performed density functional theory (DFT) calculations to understand the trends in ammonia production rates in this vacancy-ordered double perovskite system used in conjunction with g-C_3N_4. All calculations were performed to a high level of accuracy using the hybrid PBE0 functional for geometry optimization and refined by HSE06-SOC level of theory as detailed in the Computational Details section following the procedure already applied in our previous paper [26]. All alignments shown in Figure 6 were obtained from structures optimized at the PBE0 level of theory. From these structures, the absolute alignment with respect to the vacuum was corrected

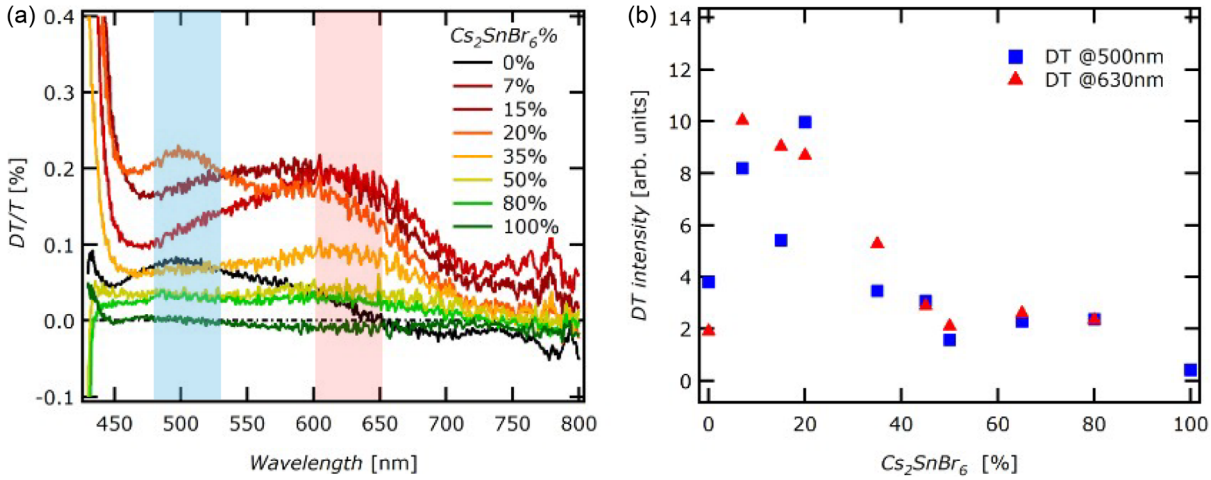

FIGURE 4 | (a) spectra extracted from DT measurements, (b) trend of DT signal extracted from different relevant wavelength regions as a function of perovskite loading.

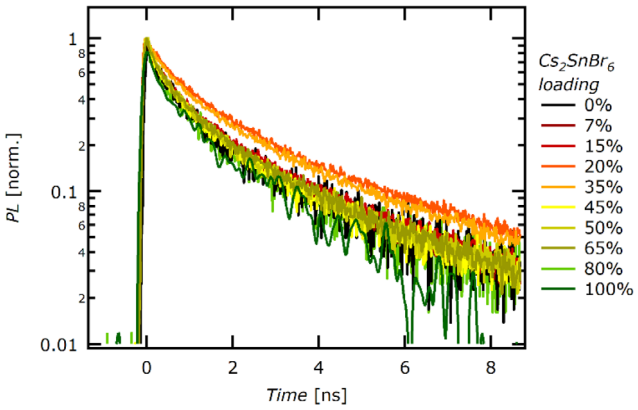

FIGURE 5 | Normalized PL time decays obtained from spectral integration of TRPL spectrograms for different compounds.

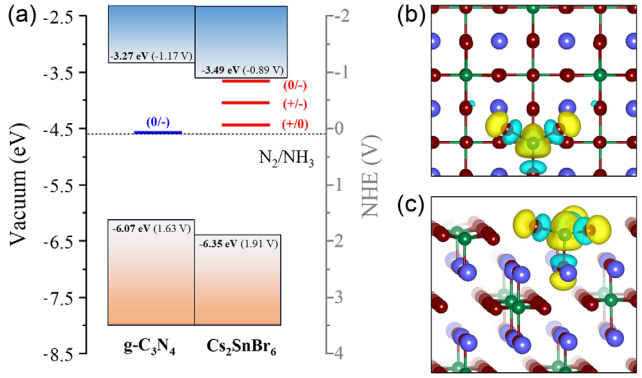

FIGURE 6 | Band alignment of g-C_3N_4 and Cs_2SnBr_6. N_2/NH_3 redox level as well as thermodynamic transition levels for the nitrogen vacancy, V_N (blue segment) and the bromide vacancy, V_{Br} (red segment) are explicitly visualized in the respective phases. (a) all the values are referred to the vacuum level as well as the electrode against NHE. (b) isodensity plot perpendicular to the 001 surface with $SnBr_2$ termination of the double perovskite of the localized state related to the neutral V_{Br}^0, resulting in the formation of an isolated Sn-tetrahedra superficial system. (c) different orientation of the vacancy ordered double perovskite motif where the clear localization on the superficial tetrahedral Sn is also reported.

using the internal potential of the bulk systems calculated at the state-of-the-art level of theory.

To analyze the NH_3 production mechanism, we started by investigating the pure vacancy-ordered double perovskite phase. As we can see from the experimental ammonia production rate in Figure 2a, this system, at 100% of perovskite, already generates a significant amount of ammonia. Recent studies have identified halide vacancies as critical defects affecting catalytic activity in analogs systems [29, 31]. However, in our previous work, we have noticed that the $Cs_2AgBiCl_6$ perovskite alone produces a very low quantity of NH_3 while Cs_2SnBr_6 results to be ≈5 time more active [26]. In contrast to $Cs_2AgBiCl_6$, Cs_2SnBr_6 shows a different defect energetics and in addition does not show effective self-trapping exciton (STE) state (see SI). This is in line with a previous study reported in literature where a very low STE was calculated [32]. In particular they identified the free exciton (FE) emission mechanism is more favorable than self-trapped exciton (STE) emission in these materials owning to their high electronic dimensionality, small effective mass, non-Jahn–Teller-like distortion, small exciton binding energy, small energy separation, small self-trapping depth, low detrapping barrier, and non-local deformation in the presence of heavy halogen [32]. The enhanced performance could be attributed to the better alignment of the band edges, particularly with respect to the transition ionization level (+/0) associated with the bromide vacancy found to be −0.067 V (NHE) very close and slightly above to the redox potential for N_2/NH_3 reported as dashed line in Figure 6. Due to the structure of the vacancy ordered perovskite, the electron is found to be localized in the superficial octahedra from where the bromide was removed to generate the defect. Our calculations predict this (+/0) transition level at 1.98 eV above the valence band maximum. The analysis of the charge density for this defect shows the presence of a localized electron that could in principle be transferred to the nitrogen starting the mechanism of photofixation. As we mentioned before, another important feature of Cs_2SnBr_6 is the lack of self-trapped electrons, visible both from photoluminescence spectra (Figure 3) as well as from theoretical calculations reported in the SI which shows the absence of emission from the distorted octahedral. This absence of STE removes extra non-radiative recombination channels, thus increasing the charge separation and the possible transfer to the defects active in the plausible mechanism of the ammonia generation. When we move to analyze the g-C_3N_4 material, we refer to already reported data by our group [26]. From the energy alignment reported in Figure 6 we can see that the g-C_3N_4/Cs_2SnBr_6 heterointerface provides the possibility of the electron injection upon photoexcitation from the perovskite conduction band (CB) to the nitrogen vacancy (V_N) of g-C_3N_4 promoting the electron trapping responsible of the initial N_2 reduction. At the same time, the electron can be trapped also by the bromide vacancy introducing additional reactive sites. To further verify the electronic structure of the heterointerface, we simulate the interacting g-C_3N_4/Cs_2SnBr_6 system reported in Figure S9, and we found that the interaction between perovskite and the carbon nitride takes place by the formation of N–Sn bond with a formation energy of 91 eV nm^{-2} confirming a very favorable interface formation tendency. In terms of the electronic properties the g-C_3N_4/Cs_2SnBr_6 interface at PBE0 (see SI), shows the same qualitative behavior of the energy level alignment reported in Figure 6 at HSE06-SOC level confirming the proposed electron transfer mechanism. The evolution of the NH_3 production with respect to the system composition results similar to that we found for $Cs_2AgBiCl_6$ but, in general, is all up-shifted in terms of absolute NH_3 production [26]. This in such way confirms that the perovskite alone already is active in producing NH_3 due to the favorable defect energy alignment, and then, when g-C_3N_4 is added, the Cs_2SnBr_6 is going to play a double role: (i) as reactive site and (ii) as light adsorber and charge generation. This aspect in conjunction with absence of STE state and the reduction of non-radiative decay led to a higher ammonia production rate. Once the carbon nitride is coupled with Cs_2SnBr_6 the ammonia generation increase is attributed to the additional charge generation upon photoexcitation that enables a better charge transfer to the nitrogen vacancy of the carbon nitride further promoting catalytic activity. On the contrary, when the quantity of perovskite is very low or absent, the carbon nitride itself does not generate a relevant amount of ammonia. As a matter of fact,

the NH_3 production mechanism promoted by Cs_2SnBr_6/g-C_3N_4 heterojunction results similar to that of $Cs_2AgBiCl_6$/g-C_3N_4 but the strategy employed here to boost the ammonia production in this novel MHP-based heterojunction was confirmed and, from a microscopic point of view, is due, mainly, to a combination of different factors such as the absence of STE state in the perovskite that reduce charge losses, and to the active role of perovskite itself in offering efficient reactive site centered at the interfacial bromide vacancy [26].

2 | Conclusions

We reported here a novel heterojunction for efficient nitrogen photofixation based on the coupling of the vacancy ordered double perovskite Cs_2SnBr_6 and carbon nitride (g-C_3N_4). The system was investigated in the whole compositional range starting from the two end members, and a clear synergistic effect between the two semiconductors was observed, reaching a maximum ammonia production rate of 266 μmol g^{-1} h^{-1} for the Cs_2SnBr_6 35 wt%/g-C_3N_4 65 wt% composition, an outstanding value obtained with no use of additional co-catalyst as noble metals. A thorough experimental and computational modeling work allowed to highlight the microscopic mechanism underpinning nitrogen reduction reaction. Graphitic carbon nitride nanosheets, through the presence of nitrogen vacancies, represent the main reaction site for nitrogen reduction with an effective charge transfer from Cs_2SnBr_6 to such active sites thanks to the formation of a type 2 heterojunction. In addition, Cs_2SnBr_6 is a very efficient semiconductor thanks to the lack of self-trapped electrons, as demonstrated by PL spectra and computational modeling work, favoring the charge carrier separation. In addition, the presence of bromide vacancies on Cs_2SnBr_6 introduces additional reactive sites and explains the efficiency in the nitrogen photofixation reaction of the perovskite alone.

The present results demonstrate the possibility of effectively employing MHP-based heterojunctions for nitrogen photofixation in addition to other well-established photoreactions such as hydrogen generation and carbon dioxide reduction. Moreover, through a wise materials engineering approach and thanks to the tunability of MHPs it is possible to design optimized systems taking advantage of their superior optoelectronic properties. The present results are extremely encouraging for the future exploitation of perovskite-based heterojunction for ammonia photogeneration, which will become a key process for the future global challenges for carbon neutrality.

Acknowledgements

A.S. acknowledges the funding PON Ricerca e Innovazione 2014–2020 REACT-EU, DM 1062 2021, project N. 04-G-14266–1. A.S., R.P., M.S acknowledge Centro Servizi Ateneo per la Ricerca (CeSAR) of University of Cagliari. R.P acknowledges PRIN 2022 CUP F53D23005090006 and PRIN 2022 F53D23001050006, funded by Italian Ministry for University and Research (MUR). M.S. acknowledges Project "Network 4 Energy Sustainable Transition—NEST", Spoke 1, Project code PE0000021, funded under the National Recovery and Resilience Plan (NRRP), Mission 4, Component 2, Investment 1.3 - MUR funded by the European Union—NextGenerationEU. M.S. acknowledges PRIN 2022 2022YM3232 – NanoPix and PRIN 2022 PNRR P2022ZYTJY—Master, funded by MUR. E.M., A.L. and L.M. acknowledge financial support under the National Recovery and Resilience Plan (NRRP), Mission 4, Component 2, Investment 1.1, Call for tender No. 104 published on 2.2.2022 by the Italian Ministry of University and Research (MUR), funded by the European Union—NextGenerationEU—Project Title 2022HRZH7P—Re-evolutionary solar fuel production envisioning water stable lead-free perovskite exploitation—REVOLUTION—CUP B53D23015350006 - Grant Assignment Decree No. 1064 adopted on 18.7.2022 by the Italian Ministry of University and Research (MUR). A.P. acknowledges financial support under the National Recovery and Resilience Plan (NRRP), Mission 4, Component 2, Investment 1.1, Call for tender No. 104 published on 2.2.2022 by the Italian Ministry of University and Research (MUR), funded by the European Union—NextGenerationEU—Project Title "Towards efficient and cost-effective nitrogen fixation via photocatalysis: insights from experiment and theory—PHOTOFIX—CUP F53D23005160006 - Grant Assignment Decree No. 1064 on 18.7.2022 by the Italian Ministry of University and Research (MUR). E.M and A.A.A wish to thank the Distinguished Scientist Fellowship Program (DSFP) of King Saud University, Riyadh, Kingdom of Saudi Arabia.

Conflicts of Interest

The authors declare no conflicts of interest.

Data Availability Statement

The data that support the findings of this study are available from the corresponding author upon reasonable request.

References

1. R. Huang, X. Li, W. Gao, et al., "Recent Advances in Photocatalytic Nitrogen Fixation: From Active Sites to Ammonia Quantification Methods," *RSC Advances* 11 (2021): 14844–14861.

2. M.-H. Vu, M. Sakar, and T.-O. Do, "Insights into the Recent Progress and Advanced Materials for Photocatalytic Nitrogen Fixation for Ammonia (NH_3) Production," *Catalysts* 8 (2018): 621.

3. X. Chen, N. Li, Z. Kong, W.-J. Ong, and X. Zhao, "Photocatalytic Fixation of Nitrogen to Ammonia: State-of-the-art Advancements and Future Prospects," *Materials Horizons* 5 (2018): 9–27.

4. A. Kumar and V. Krishnan, "Experimental Protocols for Sustainable Ammonia Production by Photocatalytic Nitrogen Fixation: Pitfalls and Remedial Measures," *Advanced Sustainable Systems* 8 (2024): 2400173.

5. M. Cheng, C. Xiao, and Y. Xie, "Photocatalytic Nitrogen Fixation: The Role of Defects in Photocatalysts," *Journal of Materials Chemistry* 7 (2019): 19616–19633.

6. D. Zhang, Y. L. Pak, X. Li et al., "Nitrogen and Oxygen Binary Vacancies Modulated g-C_3N_4/BiO_{2-x} for Visible-NIR-driven Nitrogen Photofixation," *Journal of Alloys and Compounds* 972 (2024): 172881.

7. M. Barawi, M. García-Tecedor, M. Gomez-Mendoza, et al., "Impact of $NiCo_2O_4$/$SrTiO_3$ p–n Heterojunctions on the Interface of Photoelectrochemical Water Oxidation," *ACS Applied Materials & Interfaces* 15 (2023): 53382–53394.

8. X. Wang, B. Wang, S. Yin, M. Xu, L. Yang, and H. Sun, "Highly Efficient Photocatalytic Nitrogen Fixation on Bio-inspired Triphase Interface with Improved Diffusion of Nitrogen," *Journal of Cleaner Production* 360 (2022): 132162.

9. G. Zhang, C. D. Sewell, P. Zhang, H. Mi, and Z. Lin, "Nanostructured Photocatalysts for Nitrogen Fixation," *Nano Energy* 71 (2020): 104645.

10. K. Pournemati, A. Habibi-Yangjeh, and A. Khataee, "Outstanding Photocatalytic Nitrogen Fixation Performance of TiO_2 QDs Modified by Bi_2O_3/$NaBiS_2$ Nanostructures upon Simulated Sunlight," *Journal of Colloid and Interface Science* 641 (2023): 1000–1013.

11. A. R. S. C. Lazuli, V. Ramalingam, and B. Neppolian, "Promoting Nitrogen Photofixation for the Synthesis of Ammonia using Oxygen-vacant Fe_2O_3/ZrO_2 Visible Light Photocatalyst with Straddling Heterojunction and Enhanced Charge Transfer," *Journal of Cleaner Production* 451 (2024): 142095.

12. M. Xia, B. Chong, X. Gong, et al., "Ti^{2+} Site-Promoted N≡N Bond Activation in $LaTiO_{3-x}$ Nanosheets for Nitrogen Photofixatio," *ACS Catalysis* 13 (2023): 12350–12362.

13. Y. Li, R. Li, Z. Sun, et al., "Promoted Photocatalytic N_2 Fixation to Ammonia Over Floatable TiO_2/Bi/Carbon Cloth through Relay Pathway," *Journal of Colloid and Interface Science* 664 (2024): 198–209.

14. H. Li, J. Shang, J. Shi, K. Zhao, and L. Zhang, "Facet-dependent Solar Ammonia Synthesis of BiOCl Nanosheets via a Proton-assisted Electron Transfer Pathway," *Nanoscale* 8 (2016): 1986–1993.

15. H. Li, J. Shang, Z. Ai, and L. Zhang, "Efficient Visible Light Nitrogen Fixation with BiOBr Nanosheets of Oxygen Vacancies on the Exposed {001} Facets," *Journal of the American Chemical Society* 137 (2015): 6393–6399.

16. A. Alaghmandfard and K. Ghandi, "A Comprehensive Review of Graphitic Carbon Nitride ($g\text{-}C_3N_4$)–Metal Oxide-Based Nanocomposites: Potential for Photocatalysis and Sensing," *Nanomaterials* 12 (2022): 294.

17. H. Miao, G. Zhang, X. Hu, et al., "A Novel Strategy to Prepare 2D $g\text{-}C_3N_4$ Nanosheets and their Photoelectrochemical Properties," *Journal of Alloys and Compounds* 690 (2017): 669–676.

18. J. Lee, S. H. W. Kok, B.-J. Ng, et al., "Hole Scavenger-free Nitrogen Photofixation in Pure Water with Non-metal B-doped Carbon Nitride: ImplicativeImportance of B Species for N_2 Activation," *Journal of Environmental Chemical Engineering* 11 (2023): 109511.

19. E. Vesali-Kermani, A. Habibi-Yangjeh, P. Y. Motlagh, and A. Khataee, "Enhanced Nitrogen Photofixation Performance of $g\text{-}C_3N_4$ Nanosheets Anchored with $Bi_2O_2CO_3$ and Bi_2O_3 Under Simulated Solar Light," *Journal of the Taiwan Institute of Chemical Engineers* 152 (2023): 105191.

20. L. Lin, H. Ou, Y. Zhang, and X. Wang,"Tri-s-triazine-Based Crystalline Graphitic Carbon Nitrides for Highly Efficient Hydrogen Evolution Photocatalysis," *ACS Catalysis* 6 (2016): 3921–3931.

21. R. Gupta, U. Alam, and N. Verma, "Efficient Photofixation of Nitrogen to Ammonia over an S-scheme-based $NiSnO_3$-$g\text{-}C_3N_4$ Heterojunction," *Chemical Engineering Journal* 479 (2024): 147644.

22. L. Romani and L. Malavasi, "Solar-driven Hydrogen Generation by Metal Halide Perovskites: Materials, Approaches, and Mechanistic View," *ACS Omega* 5 (2020): 25511–25519.

23. B.-M. Bresolin, Y. Park, and D. W. Bahnemann, "Recent Progresses on Metal Halide Perovskite-based Material as Potential Photocatalyst," *Catalysts* 10 (2020): 709.

24. H. Huang, B. Pradhan, J. Hofkens, M. B. J. Roeffaers, and J. A. Steele, "Solar-driven Metal Halide Perovskite Photocatalysis: Design, Stability, and Performance," *ACS Energy Letters* 5 (2020): 1107–1123.

25. J. Yuan, H. Liu, S. Wang, and X. Li, "How to Apply Metal Halide Perovskites to Photocatalysis: Challenges and Development," *Nanoscale* 13 (2021): 10281.

26. C. Tedesco, L. Gregori, A. Simbula, et al., "Reaction Mechanism of Hydrogen Generation and Nitrogen Fixation at Carbon Nitride/Double Perovskite Heterojunctions," *Advanced Energy & Sustainability Research* 5 (2024): 2400040.

27. S. Bonomi, M. Patrini, G. Bongiovanni, and L. Malavasi, "Versatile Vapor Phase Deposition Approach to Cesium Tin Bromide Materials $CsSnBr_3$, $CsSn_2Br_5$ and Cs_2SnBr_6," *RSC Advances* 10 (2020): 28478–28482.

28. G. Dong, W. Ho, and C. Wang, "Selective Photocatalytic N_2 Fixation Dependent on gC_3N_4 Induced by Nitrogen Vacancies," *Journal of Materials Chemistry A* 3 (2015): 23435–23441.

29. J. Wang, M. Zhang, Z. Chen, L. Li, G. Jiang, and Z. Li, "Enabling Enhanced Photocatalytic Hydrogen Evolution in Water by Doping Cs_2SnBr_6 Perovskite with Pt," *ACS Energy Letters* 9 (2024): 653–661.

30. A. Sharma, M. Varshney, K. H. Chae, and S. O. Won, "Mechanistic Investigations on Emission Characteristics from $g\text{-}C_3N_4$, $g\text{-}C_3N_4$@ Pt and $g\text{-}C_3N_4$@ Ag Nanostructures using X-ray Absorption Spectroscopy," *Current Applied Physics* 18 (2018): 1458–1464.

31. Z. He, Q. Tang, X. Liu, X. Yan, K. Li, and D. Yue, "Lead-Free $Cs_2AgBiBr_6$ Perovskite with Enriched Surface Defects for Efficient Photocatalytic Hydrogen Evolution," *Energy Fuels* 35 (2021): 15005–15009.

32. Z. Gao, P. Lyu, C. Xu, and L. Sun, "Enhanced Free-exciton Luminescence in $Cs_2SnBr_{6-x}I_x$: A First-principles Study," *Chemical Engineering Journal* 458 (2023): 141533.

Supporting Information

Additional supporting information can be found online in the Supporting Information section.